Preprints of the 21st IFAC World Congress (Virtual)
Berlin, Germany, July 12-17, 2020

Model-Based Control of a Pendulum by a 3-DoF Cable Robot Using Exact Linearization

Marcus Hamann * **David Winter** * **Christoph Ament** *

* *Faculty of Applied Computer Science, University of Augsburg, 86159 Augsburg, Germany (e-mail: marcus.hamann@informatik.uni-augsburg.de).*

Abstract: In this paper we present the modeling and control of a pendulum by a cable robot. The control is based on an exact linearization of the nonlinear MIMO system. The resulting closed-loop system is subsequently extended by a pendulum damping. The pose of the pendulum is determined by the connection point of the cables at the pendulum and a reflector at the end of the pendulum. Due to the model-based control and the capability of an external absolute measurement of the reflector by means of laser trackers, a high positioning accuracy is achievable, which is unique in the field of cable robots.

Keywords: robotics, cable robot, modeling, lagrangian mechanics, control, exact linearization, pendulum damping

1. INTRODUCTION

Cable-driven parallel robots (hereinafter referred to as *cable robots*) are becoming more and more popular in research. Their flexible structure and modularity allows them to carry heavy loads in a large working area where serial robots are unsuitable.

However, this large workspace also has disadvantages in terms of control precision. Suitable calibration strategies are necessary to provide a certain precision and accuracy for the cable robot. Due to measurement inaccuracies or manufacturing tolerances, the presented robot will never achieve an accuracy that would be needed for industrial applications. Therefore, a control strategy must be developed which provides a high accuracy, based on the given sensors. This accuracy can be applied, for example, to perform pick-and-place operations.

The calibration strategy presented by Hamann et al. (2019) makes it feasible to calibrate not only the cable robot but also the measuring system – a laser tracker. Since both systems are parallel kinematics, the inverse kinematics used for the underlying optimization are quite similar. In addition, we take advantage of the fact that both systems have a modular structure and that we can perform the static parameter identification module by module.

The modular sensor system consists of four laser trackers. Each tracker consists of two galvanometer scanners. The mirrors mounted on the motors deflect the laser beam. After calibration based on four laser beam path lengths, this measuring system provides an absolute position of a retroreflector in realtime. The measured values generated by the laser tracker are relative laser beam path lengths determined by an interferometer.

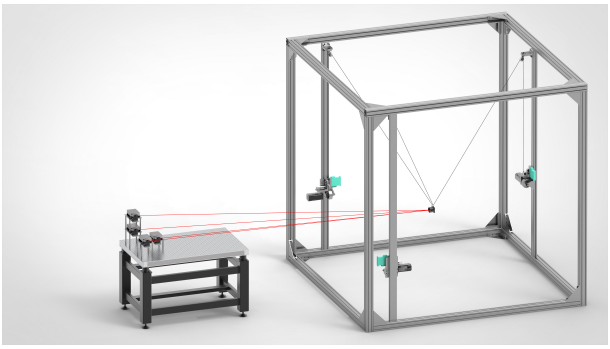

Fig. 1. System consisting of laser tracker and cable robot

The cable robot is also a modular system which consists of three modules. Each of these modules actuates one cable. With the cables connected to the endeffector, three modules form an entire system with up to 3 DoF. Fig. 1 shows an overview of the system consisting of four laser trackers (left) and the cable robot with three cables (right). As it can be seen in the figure, the endeffector of the robot is connected to a retroreflector which can be tracked by the laser trackers. In this way, the two systems are optically and mechanically connected to each other at the endeffector, allowing to perform an absolute position determination and a position control.

However, while positioning the endeffector, the reflector will start to swing which is undesirable for applications such as pick-and-place. Therefore, a precise position control is beeing designed in this work. Furthermore, a pendulum damping approach is beeing implemented to stabilize the pendulum in its equilibrium state.

1.1 State of the Art

In terms of controller design, the research area of cable robots focuses on two fields: force control of the cables and pose control of the platform. Since the focus of this work is on position control, a brief insight into the current state of research will be given.

The control of the prototype *SEGESTA* based on cable lengths (motions control in joint space) followed by the control of the cartesian coordinates (motion control in operational space) was introduced by Fang (2005). This approach features PD controllers and sets the goal of a position control which also achieves an optimum cable force distribution.

The system *CABLEV* is a kinematically underconstrained cable robot with movable cable exit points. Heyden et al. (2002) and Maier and Woernle (2003) established a feed forward control by identifying flat outputs of the model. The compensation of the pendulum motion of the platform is discussed by Heyden et al. (2002). The implementation of this is done by controlling a linearized model of pendulum motion by linear state feedback. Several years later the system was extended by Heyden and Woernle (2006) by a tracking control. All three publications mentioned above are showing simulative results. A test on the real system was done by Woernle (2013). Tracking errors of under 4 cm for the horizontal, 1 cm for the vertical and 2° for the rotary axis can be achieved. There is also a permanent control error in two of three control variables. Stoltmann et al. (2019a) and Stoltmann et al. (2019b) extend the idea of a flatness based feed forward control to a similar system, but driven by four instead of three cables in simulation.

In Yingjie et al. (2006) the control of *FAST* (Five-hundred-meter Aperture Spherical Radio Telescope) is presented. The prototype consists of two platforms. At the upper platform the cables are guided by pulleys. The cables sag due to their weight and length. The upper platform is controlled by two PID controllers, one for the position of the platform and the cable forces and one for the orientation of the platform. The lower platform is connected to the upper platform by a Stewart platform. A PID controller is also used for the lower platform. Absolute measuring laser trackers were used to determine the pose of the upper platform and the centers of both platforms. The results are validated on a replica with external dimensions of $50\,\mathrm{m} \times 50\,\mathrm{m} \times 12\,\mathrm{m}$. The lower platform can be moved with a position error of maximum 2.55 mm and an orientation error of maximum 8.45×10^{-3} rad. In Zi et al. (2008) the controller concept of FAST is extended by a fuzzy control to compensate external disturbances. In Li and Li (2019) a trajectory planning is tested on the real structure.

Alp and Agrawal (2002) are aiming to design a controller that asymptotically stabilizes a cable robot. For this purpose, a Lyaponov-based PD controller is designed. A similar intention is also followed by Kino et al. (2007), with the difference that the designed controller is robust towards incorrectly determined cable exit points and cable length measurements. Oh and Agrawal (2004) are designing a sliding mode controller, which considers workspace restrictions and guarantees stability. The design is done on a theoretical basis. A control law with the same structural design which considers feasible reference signals is formulated by Oh and Agrawal (2006).

Khosravi et al. (2013) are introducing a PID controller in combination with a cable force controller for a planar cable robot with the objective of keeping the cables under tension at all times. The control loop is cascaded.

Dallej et al. (2012) are introducing a vision-based control of a cable robot. By Dallej et al. (2019) this concept is tested on a cable robot with a very large working area ($15\,\mathrm{m} \times 10\,\mathrm{m} \times 6\,\mathrm{m}$). The sagging of cables is also considered. In addition, an overview of existing and actually tested control concepts is presented, which compares the approaches with regard to their workspace, their repeatability and payload.

Begey et al. (2019) are introducing a computed torque approach for cable robots with flexible cables. The control results are validated on a planar cable robot with three cables. The workspace is specified with an area of $1.2\,\mathrm{m} \times 0.96\,\mathrm{m}$. The endeffector is moved on a square path with an edge length of 0.2 m and a speed of $0.11\,\mathrm{m\,s^{-1}}$. There is a mean square position error of 1.7 mm and a mean square angular error of 7.8×10^{-3} rad measured by a camera system.

The approaches presented above were validated on real prototypes. There are other approaches that have been simulatively tested and are not presented here.

1.2 Objective

Based on the existing work of other institutions the following objectives were addressed in this work:

- A positioning accuracy of far less than 1 mm is to be achieved in order to ensure adequate accuracy for a pick-and-place application.
- The robot is capable of moving on trajectories with a length of several decimeters.
- An active pendulum damping is to be realized in order to affect the positioning as less as possible.

To achieve this, the model of the cable robot with and without a pendulum equipped is presented in section 2. In section 3 a controller for the connection point of the cables at the platform is designed. A pendulum damping controller is also proposed. In the following, both approaches will be combined. Section 4 shows the results and section 5 an experimental robustness analysis of the positioning and pendulum damping. In section 6 a conclusion is drawn.

2. MODELING

In the following section the modelling of the cable robot is presented. In section 2.1, the dynamics of the connection point are first modelled, followed by section 2.2, where the spherical pendulum is modelled.

2.1 3-DoF cable robot

For a 3-DoF model of the cable robot, the dynamics can be expressed as a nonlinear state space model

$$\begin{aligned} \dot{\boldsymbol{x}} &= \boldsymbol{a}(\boldsymbol{x}) + \boldsymbol{B}(\boldsymbol{x})\boldsymbol{u} \\ \boldsymbol{y} &= \boldsymbol{c}(\boldsymbol{x}) \end{aligned} \tag{1}$$

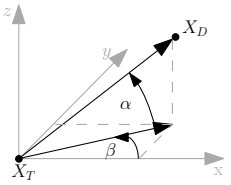

Fig. 2. Geometric relationship between the connection point $\boldsymbol{X}_T$, the detachment point $\boldsymbol{X}_D$ and the two angles θ and φ

with state vector $\boldsymbol{x}$ which represents the connection point $\boldsymbol{X}_T = [x\ y\ z]^T$ of the cables at the platform and its velocity. It is defined as

$$\boldsymbol{x} = [x\ y\ z\ v_x\ v_y\ v_z]^T\,. \tag{2}$$

The system matrix is given by

$$\boldsymbol{a}(\boldsymbol{x}) = [\dot{x}\ \dot{y}\ \dot{z}\ 0\ 0\ -g]^T\,. \tag{3}$$

The input vector

$$\boldsymbol{u} = [F_1\ F_2\ F_3]^T \tag{4}$$

corresponds to three cable forces. The input matrix can be noted as

$$\boldsymbol{B}(\boldsymbol{x}) = \begin{bmatrix} 0 & 0 & 0 \\ 0 & 0 & 0 \\ 0 & 0 & 0 \\ \frac{1}{m}\cdot \mathrm{c}\alpha_1 \cdot \mathrm{c}\beta_1 & \frac{1}{m}\cdot \mathrm{c}\alpha_2 \cdot \mathrm{c}\beta_2 & \frac{1}{m}\cdot \mathrm{c}\alpha_3 \cdot \mathrm{c}\beta_3 \\ \frac{1}{m}\cdot \mathrm{c}\alpha_1 \cdot \mathrm{s}\beta_1 & \frac{1}{m}\cdot \mathrm{c}\alpha_2 \cdot \mathrm{s}\beta_2 & \frac{1}{m}\cdot \mathrm{c}\alpha_3 \cdot \mathrm{s}\beta_3 \\ \frac{1}{m}\cdot \mathrm{s}\alpha_1 & \frac{1}{m}\cdot \mathrm{s}\alpha_2 & \frac{1}{m}\cdot \mathrm{s}\alpha_3 \end{bmatrix} \tag{5}$$

where θ_i corresponds to the elevation angle and φ_i to the azimuth angle of the i-th cable. These angles are determined by the vector from the connection point $\boldsymbol{X}_T$ to the detachment point $\boldsymbol{X}_D$ of the cable at the pulley. They are dependent on the state vector and are calculated as follows

$$\begin{aligned} \alpha_i(\boldsymbol{x}) &= \operatorname{atan2}\left(d_{i,z}, \sqrt{(d_{i,x})^2 + (d_{i,y})^2}\right), \\ \beta_i(\boldsymbol{x}) &= \operatorname{atan2}\left(d_{i,y}, d_{i,x}\right) \end{aligned} \tag{6}$$

with

$$\begin{aligned} d_{i,x} &= \boldsymbol{X}_{D_{x,i}} - x \\ d_{i,y} &= \boldsymbol{X}_{D_{y,i}} - y \\ d_{i,z} &= \boldsymbol{X}_{D_{z,i}} - z\,. \end{aligned} \tag{7}$$

Fig. 2 shows the geometric relationship between the connection point $\boldsymbol{X}_T$, the detachment point $\boldsymbol{X}_D$ and the two angles θ and φ exemplarily for one cable. If it is assumed that the position of the connection point can be measured or estimated, the output matrix reads as follows

$$\boldsymbol{c}(\boldsymbol{x}) = \boldsymbol{X}_T = [x\ y\ z]^T\,. \tag{8}$$

2.2 Spherical Pendulum

For the following model the cable robot is extended by a pendulum of length $l = \|r_2\|$. Fig. 3 shows the extended endeffector in detail. The model consists of two masses m_1 and m_2. In the following, the equations of motion are determined by means of the Lagrangian mechanics. The generalized coordinates used for this are as follows

$$\boldsymbol{q} = [x\ y\ z\ \theta\ \varphi]^T\,. \tag{9}$$

The components x, y and z correspond to the Cartesian coordinates of the connection point $\boldsymbol{X}_T$ or the vector of mass point m_1 respectively. The angles θ and φ correspond to the rotation angles around the coordinate axes y and x, respectively. Fig. 3 shows these angles for a concrete example.

In the literature the spherical pendulum is commonly modeled with the help of spherical coordinates (see Olsson (1981)). These angles correspond to the rotation around the y-axis and around the z-axis. This results in a singularity in the equations of motion, which would lead to an infinitely high angular velocity when rotating around the z-axis in the equilibrium state.

Subsequently, the direction vectors r_1 and r_2 are determined by

$$\boldsymbol{r}_1 = \begin{bmatrix} x \\ y \\ z \end{bmatrix} \tag{10}$$

and

$$\boldsymbol{r}_2 = \begin{bmatrix} x + l\cdot\sin\theta\cdot\cos\varphi \\ y + l\cdot\sin\varphi \\ z - l\cdot\cos\theta\cdot\cos\varphi \end{bmatrix}\,. \tag{11}$$

The time derivatives of the direction vectors are

$$\dot{\boldsymbol{r}}_1 = \begin{bmatrix} \dot{x} \\ \dot{y} \\ \dot{z} \end{bmatrix} \tag{12}$$

and

$$\dot{\boldsymbol{r}}_2 = \begin{bmatrix} \dot{x} + l\cdot\cos\theta\cdot\cos\varphi\cdot\dot{\theta} - l\cdot\sin\theta\cdot\sin\varphi\cdot\dot{\varphi} \\ \dot{y} + l\cdot\cos\varphi\cdot\dot{\varphi} \\ \dot{z} + l\cdot\cos\theta\cdot\sin\varphi\cdot\dot{\varphi} + l\cdot\sin\theta\cdot\cos\varphi\cdot\dot{\theta} \end{bmatrix}\,. \tag{13}$$

The generalized forces affecting the point masses can be formulated for the i-th direction vector and the j-th generalized coordinate as

$$Q_j = \sum_{i=1}^{N} \boldsymbol{F}_i \cdot \frac{\partial \boldsymbol{r}_i}{\partial q_j}\,. \tag{14}$$

For each point mass or direction vector respectively follows

$$\boldsymbol{Q}_{r_1} = \begin{bmatrix} F_x \\ F_y \\ F_z \end{bmatrix} \tag{15}$$

and

$$\boldsymbol{Q}_{r_2} = \begin{bmatrix} 0 \\ 0 \end{bmatrix}\,. \tag{16}$$

For the kinematic structure the kinetic energy T and potential energy V results to

$$T = \frac{1}{2}\cdot m_1 \cdot \left(\dot{\mathbf{r}}_1^T \cdot \dot{\mathbf{r}}_1\right) + \frac{1}{2}\cdot m_2 \cdot \left(\dot{\mathbf{r}}_2^T \cdot \dot{\mathbf{r}}_2\right) \tag{17}$$

and

$$V = m_1 \cdot g \cdot r_{1,z} + m_2 \cdot g \cdot r_{2,z}\,, \tag{18}$$

where $r_{i,z}$ is the z component of the i-th direction vector. The Lagrangian in general is

$$L = T - V \tag{19}$$

and the Lagrange's equation for the j-th generalized coordinate is

$$\frac{d}{dt}\frac{\partial L}{\partial \dot{q}_j} - \frac{\partial L}{\partial q_j} - Q_j = 0\,. \tag{20}$$

Thus, five equations of motion result. For reasons of clarity, notation is omitted here. The general structure of the equations is

Fig. 3. x-z view (left) and y-z view (right) of spherical pendulum

$$\begin{aligned}
\ddot{x} &= f(\varphi, \dot{\varphi}, \ddot{\varphi}, \theta, \dot{\theta}, \ddot{\theta}, F_x) \\
\ddot{y} &= f(\varphi, \dot{\varphi}, \ddot{\varphi}, F_y) \\
\ddot{z} &= f(\varphi, \dot{\varphi}, \ddot{\varphi}, \theta, \dot{\theta}, \ddot{\theta}, F_z) \\
\ddot{\theta} &= f(\varphi, \dot{\varphi}, \theta, \dot{\theta}, \ddot{x}, \ddot{z}) \\
\ddot{\varphi} &= f(\varphi, \theta, \dot{\theta}, \ddot{x}, \ddot{y}, \ddot{z})\,.
\end{aligned} \tag{21}$$

3. CONTROL

In section 3.1, the connection point $\boldsymbol{X}_T$ is controlled using the exact linearization approach. Subsequently, in section 3.2, a controller for pendulum damping is designed. Finally, in section 3.3, both approaches are combined.

3.1 Exact Linearization

A controller design based on an exact linearization is described by Isidori (2002), Adamy (2018) and Föllinger (1993). This will be the basis of the design in the following.

For the cable robot as *MIMO* (Multiple Input Multiple Output) system the following approach of a state space representation with n states and m inputs can be assumed.

$$\begin{aligned}
\dot{\boldsymbol{x}} &= \boldsymbol{a}(\boldsymbol{x}) + \textstyle\sum_{i=1}^{m} \boldsymbol{b}_i(\boldsymbol{x}) u_i \\
\boldsymbol{y} &= \boldsymbol{c}(\boldsymbol{x})
\end{aligned} \tag{22}$$

This notation is equivalent to the formulation of equation (1) with $u_i = F_i$ where F_i correspond to the force in the i-th cable. Matrix $\boldsymbol{c}(\boldsymbol{x})$ is equivalent to equation (8). The number of inputs and outputs are equal. This is a requirement for the design.

The connection point $\boldsymbol{X}_T$ is determined by the direct kinematics of the cable robot. After a successful calibration, as presented by Hamann (2018) and Hamann et al. (2019), both the positions of the pulleys and the cable lengths are known. Further, the direct kinematics is realized by an Extended Kalman Filter and will not be discussed here. In this way the connection point $\boldsymbol{X}_T$ can be used as an output variable.

The required output y_i with $i = 1 \dots m$ and its derivatives with respect to time are in general

$$\begin{aligned}
y_i &= c_i(\boldsymbol{x}) \\
\dot{y}_i &= L_{\boldsymbol{a}} c_i(\boldsymbol{x}) + \textstyle\sum_{k=1}^{m} L_{\boldsymbol{b}_k} c_i(\boldsymbol{x}) u_k \\
\ddot{y}_i &= L_{\boldsymbol{a}}^2 c_i(\boldsymbol{x}) + \textstyle\sum_{k=1}^{m} L_{\boldsymbol{b}_k} L_{\boldsymbol{a}} c_i(\boldsymbol{x}) u_k \\
&\vdots \\
y_i^{(\delta_i - 1)} &= L_{\boldsymbol{a}}^{\delta_i - 1} c_i(\boldsymbol{x}) + \textstyle\sum_{k=1}^{m} L_{\boldsymbol{b}_k} L_{\boldsymbol{a}}^{\delta_i - 2} c_i(\boldsymbol{x}) u_k \\
y^{(\delta)} &= L_{\boldsymbol{a}}^{\delta_i} c_i(\boldsymbol{x}) + \textstyle\sum_{k=1}^{m} L_{\boldsymbol{b}_k} L_{\boldsymbol{a}}^{\delta_i - 1} c_i(\boldsymbol{x}) u_k
\end{aligned}$$

with

$$L_{\boldsymbol{f}} h(\boldsymbol{x}) = \frac{\partial h(\boldsymbol{x})}{\partial \boldsymbol{x}} \boldsymbol{f}(\boldsymbol{x})\,. \tag{23}$$

In MIMO case, the term

$$\tilde{y}^{(\delta)} = \sum_{k=1}^{m} L_{\boldsymbol{b}_k} L_{\boldsymbol{a}}^{\delta_i - 1} c_i(\boldsymbol{x}) u_k \tag{24}$$

of the last equation becomes unequal to zero. The degree of derivative of y is called relative degree δ. The term for the delta-times derivative of y with respect to time can be noted compactly in vectorial notation as

$$\mathring{\boldsymbol{y}} = \mathring{\boldsymbol{c}}(\boldsymbol{x}) + \boldsymbol{D}(\boldsymbol{x}) \cdot u \tag{25}$$

with

$$\mathring{\boldsymbol{y}} = \begin{bmatrix} y^{(\delta_1)} \\ y^{(\delta_2)} \\ \vdots \\ y^{(\delta_m)} \end{bmatrix}, \tag{26}$$

$$\mathring{\boldsymbol{c}}(\boldsymbol{x}) = \begin{bmatrix} L_{\boldsymbol{a}}^{\delta_1} c_1(\boldsymbol{x}) \\ L_{\boldsymbol{a}}^{\delta_2} c_2(\boldsymbol{x}) \\ \vdots \\ y L_{\boldsymbol{a}}^{\delta_m} c_m(\boldsymbol{x}) \end{bmatrix} \tag{27}$$

and

$$\boldsymbol{D}(\boldsymbol{x}) = \begin{bmatrix} L_{\boldsymbol{b}_1} L_{\boldsymbol{a}}^{\delta_1 - 1} c_1(\boldsymbol{x}) & L_{\boldsymbol{b}_2} L_{\boldsymbol{a}}^{\delta_1 - 1} c_1(\boldsymbol{x}) & \dots & L_{\boldsymbol{b}_m} L_{\boldsymbol{a}}^{\delta_1 - 1} c_1(\boldsymbol{x}) \\ L_{\boldsymbol{b}_1} L_{\boldsymbol{a}}^{\delta_2 - 1} c_2(\boldsymbol{x}) & L_{\boldsymbol{b}_2} L_{\boldsymbol{a}}^{\delta_2 - 1} c_2(\boldsymbol{x}) & \dots & L_{\boldsymbol{b}_m} L_{\boldsymbol{a}}^{\delta_2 - 1} c_2(\boldsymbol{x}) \\ \vdots & \vdots & \ddots & \vdots \\ L_{\boldsymbol{b}_1} L_{\boldsymbol{a}}^{\delta_m - 1} c_m(\boldsymbol{x}) & L_{\boldsymbol{b}_2} L_{\boldsymbol{a}}^{\delta_m - 1} c_m(\boldsymbol{x}) & \dots & L_{\boldsymbol{b}_m} L_{\boldsymbol{a}}^{\delta_m - 1} c_m(\boldsymbol{x}) \end{bmatrix} \tag{28}$$

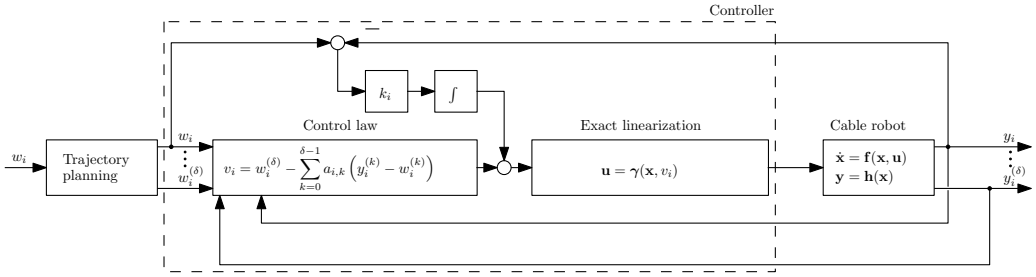

Fig. 4. Exact linearization of one output y_i with trajectory planning, tracking control and output-feedback control

For the cable robot the vectorial relative degree (relative degree for each output) is

$$\boldsymbol{\delta} = \begin{bmatrix}\delta_1\\ \delta_2\\ \delta_3\end{bmatrix} = \begin{bmatrix}2\\ 2\\ 2\end{bmatrix}. \tag{29}$$

The vector-valued functions $\overset{\circ}{\boldsymbol{c}}(\boldsymbol{x})$ and $\boldsymbol{D}(\boldsymbol{x})$ result in

$$\overset{\circ}{\boldsymbol{c}}(\boldsymbol{x}) = \begin{bmatrix}0\\ 0\\ -g\end{bmatrix} \tag{30}$$

and

$$\boldsymbol{D}(\boldsymbol{x}) = \frac{1}{m}\begin{bmatrix}\mathrm{c}(\alpha_1)\cdot\mathrm{c}(\beta_1) & \mathrm{c}(\alpha_2)\cdot\mathrm{c}(\beta_2) & \mathrm{c}(\alpha_3)\cdot\mathrm{c}(\beta_3)\\ \mathrm{c}(\alpha_1)\cdot\mathrm{s}(\beta_1) & \mathrm{c}(\alpha_2)\cdot\mathrm{s}(\beta_2) & \mathrm{c}(\alpha_3)\cdot\mathrm{s}(\beta_3)\\ \mathrm{s}(\alpha_1) & \mathrm{s}(\alpha_2) & \mathrm{s}(\alpha_3)\end{bmatrix}. \tag{31}$$

By rearranging equation (25), the control law results in

$$\boldsymbol{u}_x = -\boldsymbol{D}^{-1}(\boldsymbol{x})\overset{\circ}{\boldsymbol{c}}(\boldsymbol{x}) + \boldsymbol{D}^{-1}(\boldsymbol{x})\boldsymbol{v}\,. \tag{32}$$

with

$$\boldsymbol{v} = \boldsymbol{K}_x\boldsymbol{z}\,, \tag{33}$$

$$\boldsymbol{K}_x = (\lambda_1 \ldots \lambda_n) \tag{34}$$

and

$$z_i = L_{\boldsymbol{a}}^{\delta_i-1}c_i(\boldsymbol{x})\,. \tag{35}$$

The eigenvalues λ_i can be chosen according to the desired dynamics. The control signal $\boldsymbol{u}$ consists of a feedforward control

$$\boldsymbol{r}(\boldsymbol{x}) = \boldsymbol{D}^{-1}(\boldsymbol{x})\overset{\circ}{\boldsymbol{c}}(\boldsymbol{x}) \tag{36}$$

and a feedback control

$$\boldsymbol{M}(\boldsymbol{x}) = \boldsymbol{D}^{-1}(\boldsymbol{x})\boldsymbol{v}\,. \tag{37}$$

At this point it is essential that matrix $\boldsymbol{D}(\boldsymbol{x})$ is invertible. For the invertibility the following must apply

$$\det\boldsymbol{D}(\boldsymbol{x}) \neq 0\,. \tag{38}$$

Therefore, the column vectors of the matrix from equation (31) must be linearly independent. Since the column vectors correspond to the acceleration vectors of the cables, this condition is only fulfilled for geometrically feasible configurations.

This completes the design of an exact linearization via feedback. The input output behaviour of the controlled system is now linear. Each reference variable w_i affects the corresponding output variable y_i through a transfer function $G_i(s) = \frac{Y_i(s)}{W_i(s)}$. The coefficients of the transfer function affect the dynamics of the controlled system and can be specified in several ways. A simple way to do this is a pole placement. In that way, we are able to define linear dynamics for each output (components of the vector $\boldsymbol{X}_T$) and the control law can be implemented. At this point, however, some improvements have been made. These include

- a *trajectory planning* to avoid step changes of the reference signal,
- a *tracking control* reducing tracking errors,
- an *output-feedback control* to compensate for permanent control errors.

Trajectory Planning The trajectory planning is based on a cubic polynomial trajectory for the reference position (see Spong (2012)). This results in a quadratic profile of the velocity and a linear profile of the acceleration. In this way a continuous dynamic can be specified. A concrete profile is shown in the results.

Tracking Control The characteristic polynomial – resulting from the eigenvalues of equation (34) – transformed into the laplace plane reads

$$\frac{Y_i(s)}{W_i(s)} = \frac{v_{i,0}}{s^{\delta_i} + a_{i,\delta_i-1}s^{\delta_i-1} + a_{i,\delta_i-2}s^{\delta_i-2} + \ldots + a_{i,0}}\,. \tag{39}$$

This transfer function determines the dynamics for the controlled system. In case of an ideal tracking control, this transfer function reads

$$\frac{Y_i(s)}{W_i(s)} \overset{!}{=} 1\,. \tag{40}$$

That means the numerator of the transfer function must be extended by the coefficients of the denumerator.

$$\frac{Y_i(s)}{W_i(s)} = \frac{s^{\delta_i} + v_{i,\delta_i-1}s^{\delta_i-1} + v_{i,\delta_i-2}s^{\delta_i-2} + \ldots + v_{i,0}}{s^{\delta_i} + a_{i,\delta_i-1}s^{\delta_i-1} + a_{i,\delta_i-2}s^{\delta_i-2} + \ldots + a_{i,0}} \tag{41}$$

Output-Feedback Control Due to stick-slip, the control error is not zero. Therefore, an additional integrator is implemented, which integrates the residual control error and adds it to the system as an additional control signal. Fig. 4 shows the resulting block diagram including exact linearization of one output y_i, extended by a trajectory planning, tracking control and output-feedback control. The entire controller is indicated by the subsystem *Controller* in Fig. 4.

3.2 Stabilization of the Pendulum

In order to stabilize the pendulum, the set of differential equations (21) were used. These were linearized in the stable equilibrium according to

$$\begin{aligned}\boldsymbol{A}_p &= \left.\frac{\partial \boldsymbol{f}_p}{\partial \boldsymbol{x}_p}\right|_{\boldsymbol{x}_e,\boldsymbol{u}_e}\\ \boldsymbol{B}_p &= \left.\frac{\partial \boldsymbol{f}_p}{\partial \boldsymbol{u}_p}\right|_{\boldsymbol{x}_e,\boldsymbol{u}_e}\end{aligned} \tag{42}$$

with

$$\begin{aligned} \boldsymbol{f}_p &= \begin{bmatrix} \dot{x} & \dot{y} & \dot{z} & \dot{\theta} & \dot{\varphi} & \ddot{x} & \ddot{y} & \ddot{z} & \ddot{\theta} & \ddot{\varphi} \end{bmatrix}^T \\ \boldsymbol{x}_p &= \begin{bmatrix} x & y & z & \theta & \varphi & \dot{x} & \dot{y} & \dot{z} & \dot{\theta} & \dot{\varphi} \end{bmatrix}^T \\ \boldsymbol{u}_p &= \begin{bmatrix} F_x & F_y & F_z \end{bmatrix}^T \end{aligned} \tag{43}$$

The resulting linear state space model

$$\dot{\boldsymbol{x}}_p = \boldsymbol{A}_p \boldsymbol{x}_p + \boldsymbol{B}_p \boldsymbol{u}_p \tag{44}$$

can now be controlled with a linear-quadratic regulator (LQR). This results in a control law

$$\boldsymbol{u}_p = -\boldsymbol{K}_p \boldsymbol{x}_p \tag{45}$$

with

$$\boldsymbol{K}_p \in \mathbb{R}^{3\times 10}\,. \tag{46}$$

3.3 Coupling of Both Approaches

The exact linearization via feedback, presented in section 3.1, was designed to move the connection point precisely. The LQR introduced in section 3.2, was designed to stabilize the pendulum motion. Both approaches are beeing combined in the following. For this purpose the control signals will be superimposed. Fig. 5 shows the resulting block diagram which will be discussed in the following.

Dynamics The dynamics of the endeffector can be divided into the dynamics of the connection point and the dynamics of the pendulum. Both blocks are connected to each other by the state vector. Due to the separate control of the position of the connection point and the pendulum damping, the feedback of the pendulum dynamics on the endeffector is neglected (indicated by the dashed line). From the position controller's (see subsystem Fig. 4 and Fig. 5) point of view, the pendulum movement is a disturbance.

Measuring angles For the calculation of the pendulum angles the connection point and the reflector center are necessary. The connection point is determined by the direct kinematics of the cable robot. For each endeffector position, the detachment points of the cables and the cable lengths are given by a prior calibration. The reflector center is measured by the laser tracker. In this case, the direct kinematics of the laser trackers are used to determine the reflector center from known tracker positions and laser beam path lengths. The direct kinematics are realized by an *Extended Kalman Filter*.

Due to a non-optimal modeling and calibration of the cable robot and measurement inaccuracies of the laser trackers, the pendulum angles cannot be measured correctly. This causes the pendulum angles in the equilibrium position to be unequal to zero. Therefore, the pendulum angles are filtered by a high-pass filter. In this way, the pendulum angles become nearly zero mean. As a result, changes in the pendulum angles can still be measured accurately. The calculation for this is done in block "dynamics of the pendulum".

Control signal selection The LQR is exclusively designed to control the pendulum motion. Therefore, the states corresponding to the motion of the connection point are set to zero. The resulting control signal is $\boldsymbol{u}_p^*$.

Low-pass filter The low-pass filter is used to integrate the control signal $\boldsymbol{u}_p^*$. An integrator cannot be used because the high-pass filter applies an additional dynamics to the signal. As a result, after filtering by the high-pass filter, the pendulum angles converge to zero very slowly. By choosing suitable parameter, the low-pass filter approximately works as an integrator.

Superimposing control signals Finally, the two control signals ($\boldsymbol{u}_p^*$ and low-pass filtered $\boldsymbol{u}_p^*$) are added to the reference signals $\ddot{\boldsymbol{w}}$ and $\dot{\boldsymbol{w}}$. To avoid step changes in the reference signal due to deflection of the pendulum, nothing is added to the position reference $\boldsymbol{w}$.

Geometric feed forward control The overall aim is precise positioning of the reflector center. However, we are only able to control the connection point. The feed forward control is used to shift the set position on the basis of the known geometry of the pendulum. Errors caused by this feed forward control are compensated by an integral control with gain $k_{i,p}$. The impact of the integral control is small compared to the resulting control variables resulting from the position controller and the pendulum damping.

4. RESULTS

Fig. 6 show the reference signals resulting from trajectory planning and the errors of the control variables during movement on the given paths. The control variables are the components of the position of the reflector center. It can be seen that there is no permanent control error. We achieve a positioning accuracy of the reflector center of 15×10^{-6} m. During movement tracking errors of up to 5×10^{-3} m occur (see Fig. 6, component e_x). That means the pendulum damping as well as the position control were effective.

5. EXPERIMENTAL ROBUSTNESS ANALYSIS

The nominal parameters chosen for the design may differ from the real parameters. This includes, for example, the mass of the platform components. The platform was assumed to be composed of two masses connected by a massless rod. Therefore, robustness analyses in which these masses are varied will to be performed in the following. The analysis consists of four scenarios in which different experiments were conducted. In the first scenario, the influence of a variation on decoupling is examined. For this purpose, the mass m_1 used for the matrix $\boldsymbol{D}(\boldsymbol{x})$ is varied according to table 1. Afterwards, the RMSE (*root-mean-square error*) between the reference and the controlled variables are determined.

For pendulum damping both masses are included in the control. For scenario 2 and 3 the position controller is not changed. In scenario 2, however, the upper mass m_1 and in scenario 2 the lower mass m_2 is varied in the design of the pendulum damping. The results can be found in the tables 2 and 3. The nominal case is indicated by the factor 1.0 in the left column. All three scenarios presented up to now show an influence on the quality of the control. However, the experiments show that the mass can be varied in a wide range from 10% – 190% and the control performance is still good.

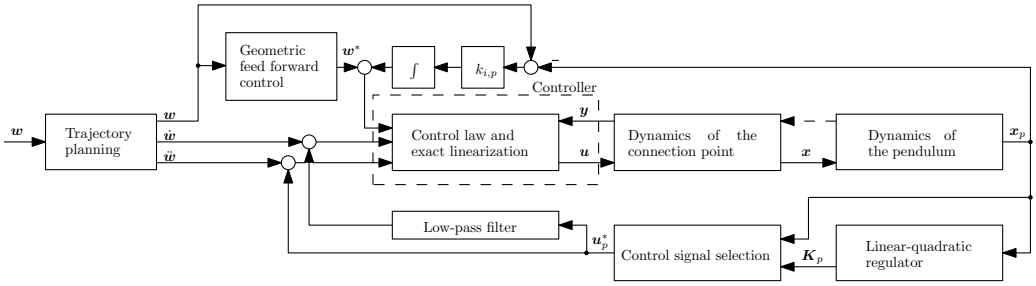

Fig. 5. Pendulum damping control including position control via exact linearization and LQR for stabilization of the pendulum

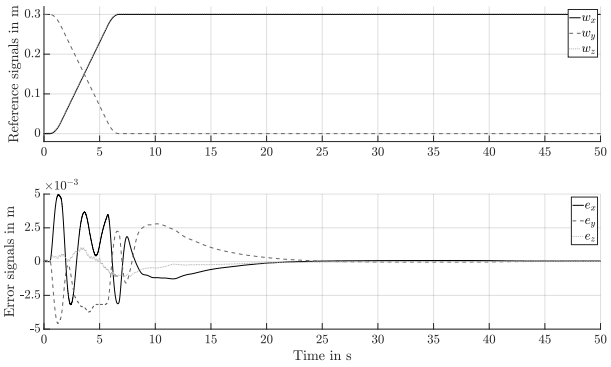

Fig. 6. Error of the x-coordinate of the reflector center

In a fourth scenario, the connection point is actuated with a sinusoidal signal. The reference distance is 0.1 m. The frequency $\tilde{f}_0$ of this signal is increased up to the resonance frequency of the pendulum. The results are shown in table 4. These results demonstrate clearly the competing behaviour of the two controllers (position and pendulum controller). For an excitation close to the resonance frequency, the connection point as well as the reflector center come to a deadlock and the controlled variable is no longer able to follow the reference variable.

Table 1. Experimental robustness scenario 1

$\tilde{m}_1$	RMSE of x	RMSE of y	RMSE of z
$0.1 \cdot m_1$	1.34×10^{-3} m	1.84×10^{-3} m	1.48×10^{-3} m
$0.5 \cdot m_1$	1.05×10^{-3} m	1.43×10^{-3} m	1.16×10^{-3} m
$0.9 \cdot m_1$	1.07×10^{-3} m	1.39×10^{-3} m	1.23×10^{-3} m
$1.0 \cdot m_1$	1.05×10^{-3} m	1.32×10^{-3} m	0.31×10^{-3} m
$1.1 \cdot m_1$	1.00×10^{-3} m	1.31×10^{-3} m	1.24×10^{-3} m
$1.5 \cdot m_1$	1.04×10^{-3} m	1.39×10^{-3} m	1.28×10^{-3} m
$1.9 \cdot m_1$	1.01×10^{-3} m	1.25×10^{-3} m	1.23×10^{-3} m

Table 2. Experimental robustness scenario 2

$\tilde{m}_1$	RMSE of x	RMSE of y	RMSE of z
$0.1 \cdot m_1$	1.12×10^{-3} m	1.37×10^{-3} m	0.44×10^{-3} m
$0.5 \cdot m_1$	1.11×10^{-3} m	1.36×10^{-3} m	1.44×10^{-3} m
$0.9 \cdot m_1$	1.23×10^{-3} m	1.35×10^{-3} m	0.43×10^{-3} m
$1.0 \cdot m_1$	1.05×10^{-3} m	1.32×10^{-3} m	0.31×10^{-3} m
$1.1 \cdot m_1$	1.12×10^{-3} m	1.34×10^{-3} m	0.43×10^{-3} m
$1.5 \cdot m_1$	1.12×10^{-3} m	1.36×10^{-3} m	1.44×10^{-3} m
$1.9 \cdot m_1$	1.12×10^{-3} m	1.37×10^{-3} m	0.45×10^{-3} m

Table 3. Experimental robustness scenario 3

$\tilde{m}_2$	RMSE of x	RMSE of y	RMSE of z
$0.1 \cdot m_2$	1.12×10^{-3} m	1.25×10^{-3} m	0.41×10^{-3} m
$0.5 \cdot m_2$	0.93×10^{-3} m	1.41×10^{-3} m	1.18×10^{-3} m
$0.9 \cdot m_2$	0.94×10^{-3} m	1.41×10^{-3} m	1.19×10^{-3} m
$1.0 \cdot m_2$	1.05×10^{-3} m	1.32×10^{-3} m	0.31×10^{-3} m
$1.1 \cdot m_2$	0.95×10^{-3} m	1.34×10^{-3} m	1.19×10^{-3} m
$1.5 \cdot m_2$	0.95×10^{-3} m	1.42×10^{-3} m	1.19×10^{-3} m
$1.9 \cdot m_2$	0.95×10^{-3} m	1.42×10^{-3} m	1.18×10^{-3} m

Table 4. Experimental robustness scenario 3

$\tilde{f}_0$	RMSE of x	RMSE of y	RMSE of z
$0.1 \cdot f_0$	0.31×10^{-3} m	0.65×10^{-3} m	0.60×10^{-3} m
$0.5 \cdot f_0$	2.32×10^{-3} m	41.60×10^{-3} m	1.07×10^{-3} m
$0.9 \cdot f_0$	2.09×10^{-3} m	67.82×10^{-3} m	2.94×10^{-3} m
$1.0 \cdot f_0$	1.50×10^{-3} m	65.54×10^{-3} m	3.10×10^{-3} m

6. CONCLUSION

In this work, we presented the modeling and control of a 3-DoF cable robot. The endeffector of the robot was extended by a pendulum. At the end of the pendulum a reflector is attached. The position of the reflector is determined in real time by laser trackers using an Extended Kalman Filter. The control objective is the precise positioning of the reflector center. The challenge is to compensate for oscillations of the pendulum.

The positioning of the connection point of the cables at the endeffector is based on an exact linearization. In order to damp oscillations of the pendulum, the control concept was extended by a LQR for control of the pendulum angles. On the basis of the geometry of the endeffector (mainly length of the pendulum), the reflector center can be positioned quite well in this way open-loop. In order to reduce the residual error, an integral controller is used.

The RMSE of the positioning of the reflector center is 15×10^{-6} m. We are able to achieve a tracking error of up to 5×10^{-3} m (see Fig. 6).

In addition, robustness analyses were carried out. For this purpose, the masses of the platform were varied in the controller design in order to analyze the influence on the control result. It turns out that the design is robust to a variation of the masses. The control result, however, depends on the given trajectory. For excitations close to the resonance frequency of the pendulum, an acceptable position control is not possible anymore.

For the future, we aim to apply the concept of exact linearization to the model of the pendulum, so that a parallel positioning and pendulum damping can be achieved.

REFERENCES

Adamy, J. (2018). *Nichtlineare Systeme und Regelungen*. Springer Vieweg, Berlin, 3., aktualisierte Auflage edition. doi:10.1007/978-3-662-55685-6.

Alp, A.B. and Agrawal, S.K. (2002). Cable suspended robots: feedback controllers with positive inputs. In *Proceedings of the 2002 American*, 815–820. doi:10.1109/ACC.2002.1024915.

Begey, J., Cuvillon, L., Lesellier, M., Gouttefarde, M., and Gangloff, J. (2019). Dynamic control of parallel robots driven by flexible cables and actuated by position-controlled winches. *IEEE Transactions on Robotics*, 35(1), 286–293. doi:10.1109/TRO.2018.2875415.

Dallej, T., Gouttefarde, M., Andreff, N., Dahmouche, R., and Martinet, P. (2012). Vision-based modeling and control of large-dimension cable-driven parallel robots. In *2012 IEEE/RSJ International Conference on Intelligent Robots and Systems (IROS 2012)*, 1581–1586. IEEE, Piscataway, NJ. doi:10.1109/IROS.2012.6385504.

Dallej, T., Gouttefarde, M., Andreff, N., Hervé, P.E., and Martinet, P. (2019). Modeling and vision-based control of large-dimension cable-driven parallel robots using a multiple-camera setup. *Mechatronics*, 61, 20–36. doi:10.1016/j.mechatronics.2019.05.004.

Fang, S. (2005). *Design, modeling and motion control of tendon-based parallel manipulators: Zugl.: Duisburg-Essen, Univ., Diss., 2005*, volume 1076 of *Fortschritt-Berichte VDI Reihe 8, Mess-, Steuerungs- und Regelungstechnik*. VDI-Verl., Düsseldorf, als ms. gedr edition.

Föllinger, O. (1993). Nichtlineare Regelungen 2: Harmonische Balance, Popow- und Kreiskriterium, Hyperstabilität, Synthese im Zustandsraum: mit 18 Übungsaufgaben mit Lösungen. doi:10.1524/9783110406146.

Hamann, M. (2018). Calibration procedure for a geometrically reconfigurable 3-dof cable-driven parallel robot. In *Modelling, Simulation and Identification*. doi:10.2316/P.2018.857-013.

Hamann, M., Nüsse, P.M., Winter, D., and Ament, C. (2019). Towards a precise cable-driven parallel robot - a model-driven parameter identification enhanced by data-driven position correction. In A. Pott and T. Bruckmann (eds.), *CABLE-DRIVEN PARALLEL ROBOTS*, volume 74 of *Mechanisms and Machine Science*, 367–376. Springer, [S.l.]. doi:10.1007/978-3-030-20751-9_31.

Heyden, T., Maier, T., and Woernle, C. (2002). Trajectory tracking control for a cable suspension manipulator. In J. Lenarčič and F. Thomas (eds.), *Advances in Robot Kinematics*, volume 19, 125–134. Springer, Dordrecht. doi:10.1007/978-94-017-0657-5_14.

Heyden, T. and Woernle, C. (2006). Dynamics and flatness-based control of a kinematically undetermined cable suspension manipulator. *Multibody System Dynamics*, 16(2), 155–177. doi:10.1007/s11044-006-9023-5.

Isidori, A. (2002). *Nonlinear control systems*. Communications and control engineering series. Springer, Berlin, 3. ed., [nachdr.] edition.

Khosravi, M.A., Taghirad, H.D., and Oftadeh, R. (2013). A positive tensions pid controller for a planar cable robot: An experimental study. In *2013 First RSI/ISM International Conference*, 325–330. doi:10.1109/ICRoM.2013.6510127.

Kino, H., Yahiro, T., Takemura, F., and Morizono, T. (2007). Robust pd control using adaptive compensation for completely restrained parallel-wire driven robots: Translational systems using the minimum number of wires under zero-gravity condition. *IEEE Transactions on Robotics*, 23(4), 803–812. doi:10.1109/TRO.2007.900633.

Li, H. and Li, M. (2019). An experimental study on control accuracy of fast cable robot following zigzag astronomical trajectory. In A. Pott and T. Bruckmann (eds.), *CABLE-DRIVEN PARALLEL ROBOTS*, volume 74 of *Mechanisms and Machine Science*, 245–253. Springer, [S.l.]. doi:10.1007/978-3-030-20751-9_21.

Maier, T. and Woernle, C. (2003). Flachheitsbasierte bahnsteuerung von seilgeführten handhabungssystemen (flatness-based control of cable suspension manipulators). *at - Automatisierungstechnik*, 51(6-2003), 265–273. doi:10.1524/auto.51.6.265.22449.

Oh, S.R. and Agrawal, S.K. (2004). Nonlinear sliding mode control and feasible workspace analysis for a cable suspended robot with input constraints and disturbances. In *Proceedings of the 2004 American Control Conference ACC*, 4631–4636 vol.5. American Automatic Control Council, Evanston, Ill and Piscataway, N.J. doi:10.23919/ACC.2004.1384041.

Oh, S.R. and Agrawal, S.K. (2006). Generation of feasible set points and control of a cable robot. *IEEE Transactions on Robotics*, 22(3), 551–558. doi:10.1109/TRO.2006.870646.

Olsson, M.G. (1981). Spherical pendulum revisited. *American Journal of Physics*, 49(6), 531–534. doi:10.1119/1.12666.

Spong, M.W. (2012). *Robot Modeling and Control*. JOHN WILEY & Sons, 2nd revised edition edition.

Stoltmann, M., Froitzheim, P., Fuchs, N., Flügge, W., and Woernle, C. (2019a). Linearised feedforward control of a four-chain crane manipulator. In A. Pott and T. Bruckmann (eds.), *CABLE-DRIVEN PARALLEL ROBOTS*, volume 74 of *Mechanisms and Machine Science*, 233–244. Springer, [S.l.]. doi:10.1007/978-3-030-20751-9_20.

Stoltmann, M., Froitzheim, P., Fuchs, N., and Woernle, C. (2019b). Flatness-based feedforward control of a crane manipulator with four load chains. In B. Corves, P. Wenger, and M. Hüsing (eds.), *EuCoMeS 2018*, volume 59 of *Mechanisms and Machine Science*, 61–68. Springer, Cham. doi:10.1007/978-3-319-98020-1_8.

Woernle, C. (2013). Trajectory tracking for a three-cable suspension manipulator by nonlinear feedforward and linear feedback control. In T. Bruckmann and A. Pott (eds.), *Cable-Driven Parallel Robots*, volume 12 of *Mechanisms and Machine Science*, 371–386. Springer, Berlin and Heidelberg. doi:10.1007/978-3-642-31988-4_23.

Yingjie, L., Wenbai, Z., and Gexue, R. (2006). Feedback control of a cable-driven gough-stewart platform. *IEEE Transactions on Robotics*, 22(1), 198–202. doi:10.1109/TRO.2005.861459.

Zi, B., Duan, B.Y., Du, J.L., and Bao, H. (2008). Dynamic modeling and active control of a cable-suspended parallel robot. *Mechatronics*, 18(1), 1–12. doi:10.1016/j.mechatronics.2007.09.004.